

A Computation-Enhanced High-Dimensional Quantum Gate for Silicon-Vacancy Spins

Gang Fan^{1,2} and Fang-Fang Du^{1*}

¹*Science and Technology on Electronic Test and Measurement Laboratory,
North University of China, Taiyuan, 030051, China*

²*Institute for Quantum Science and Technology, College of Science,
National University of Defense Technology, Changsha, 410073, China*

(Dated: September 19, 2024)

Qudit-based quantum gates in high-dimensional Hilbert space can provide a viable route towards effectively accelerating the speed of quantum computing and performing complex quantum logic operations. In the paper, we propose a 2-qudit 4×4 -dimensional controlled-not (CNOT) gate for four silicon-vacancy spins, in which the first two electron-spin states in silicon-vacancy centers are encoded as the control qudits, and the other ones as the target qudits. The proposed protocol is implemented with assistance of an ancillary photon that serves as a common-data bus linking four motionless silicon-vacancy spins placed in four independent single-sided optical nanocavities. Moreover, the CNOT gate works in a deterministic manner by performing the relational feed-forward operations corresponding to the diverse outcomes of the single-photon detectors to be directed against the ancillary photon. Further, it can be potentially generalized to other solid-state quantum system. Under current technological conditions, both the efficiency and fidelity of the 2-qudit CNOT gate are high.

I. INTRODUCTION

Quantum computing is an emerging technology that leverages the essential principles of quantum mechanics to execute computational tasks that are inefficient or intractable for classical computing [1–5]. Quantum logic gates [6, 7] enable precise manipulation of quantum qubits to facilitate the execution of specific computational tasks and play a crucial part in quantum information processing (QIP) [8, 9], where all unitary operations can be implemented with a set of universal two-qubit controlled-not (CNOT) gates and parallel one-qubit operations [10]. Consequently, the ongoing research and advancement of the CNOT gates emerge as pivotal catalysts propelling the evolution of quantum technology, i.e., a wide range of fascinating applications in entanglement concentration [11], entanglement purification [12, 13], quantum secure direct communication [14, 15], and quantum key distribution [16].

The traditional CNOT gates only perform logic operations on two-dimensional qubits, i.e., $|0\rangle$ and $|1\rangle$, and the relational transformations are $|0_c, 0_t\rangle \rightarrow |0_c, 0_t\rangle$, $|0_c, 1_t\rangle \rightarrow |0_c, 1_t\rangle$, $|1_c, 0_t\rangle \rightarrow |1_c, 1_t\rangle$, and $|1_c, 1_t\rangle \rightarrow |1_c, 0_t\rangle$. Based on the two-dimensional qubit system, a variety of quantum algorithms may be executed with the help of special quantum circuits composed of basic gates corresponding to unitary matrices and further require extensive qubits to encode information, which limit the flexibility of quantum computing to face the challenge of large-scale integration in practice. To overcome the limitation, high-dimensional quantum logic gates [17–23] that exploit high-dimensional quantum qudits to encode and process multi-valued information, have been proposed recently, thus improving the speed of quantum computing and QIP. Besides, high-dimensional systems not only are flexible with regard to improvements to the channel capacity and security requiring less resource overheads, but also improve the execution of quantum algorithms to offer enhanced computational capacity and higher computational accuracy.

Extensively and in-depth studied have been devoted to have been devoted to qubit-based CNOT gates in both theory and experiment with diverse physical systems, such as linear optics [24–26], superconducting qubits [27, 28], nuclear magnetic resonance [29, 30], atoms [31–34], color centers in diamond [35–37], and quantum dots [38–41]. Among these systems, the silicon-vacancy (SiV) center has been regarded as one of the attractive candidates to implement scalable general-purpose QIP due to excellent optical property and scalability with long coherence time. Especially, the SiV center appears a like four-level system [42–46], making it suitable for variable interesting tasks, i.e., entanglement generation of multiple SiV centers and the realization of tunable and strong coupling between photons and SiV centers located in the single quantum level. Establishing a connection between an auxiliary photon and individual spins is a fundamental requirement for the development of QIP [47]. A deterministic link can be achieved by employing nanocavity-SiV⁻ system.

In the paper, we investigate the implementation of the deterministic 2-qudit 4×4 -dimensional CNOT gate for a four- SiV system, in which both the control and target qudits are encoded on two SiV spins. An ancillary photon is

* dufangfang19871210@163.com

available for contacting and interacting with four stationary SiV spins embedded independently in four single-sided optical cavities. After that, the photon is detected by the single-photon detectors and then the SiV spins are executed the relational feed-forward operations to make the CNOT gate with unity success probability in principle.

II. AN SILICON-VACANCY CENTER

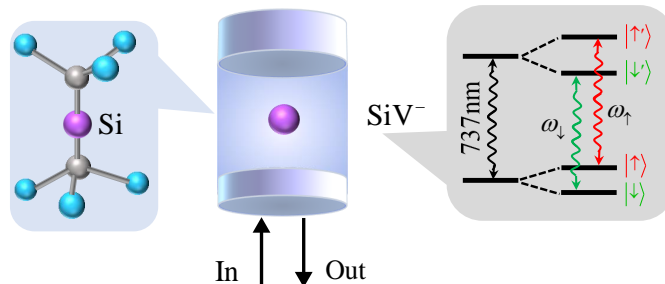


FIG. 1. (a) The coupling system involved a SiV^- center and an optical cavity; (b) The structural arrangement of energy levels and optical transitions within the SiV^- center.

A negatively charged SiV (SiV^-) center configuration placed in a single-sided nanocavity with a resonance frequency to be close to 737 nm as depicted in Figure 1. A substitutional silicon atom is located between two carbon vacancies of the SiV^- center [48–50]. The consequential D_{3d} inversion symmetry of the SiV^- center with regard to the Si atom brings about a disappearing electron-dipole moments of the excited and ground states [48], so the SiV^- center is noise-resistant, especially fixed in nanophotonic framework, and has better optical performances than a nitrogen-vacancy (NV) center facing a low temperature (lower than 500 mK) [49]. Under moderate strain, the energy levels of the SiV^- center are reduced to two spin sublevels in the ground (excited) states, i.e., $|\downarrow\rangle$ and $|\uparrow\rangle$ ($|\downarrow'\rangle$ and $|\uparrow'\rangle$), ignoring other unrelated levels due to large detunings. If an external effective magnetic field is introduced along symmetry axis of the SiV^- center, two spin-conserving transitions, i.e., $|\downarrow\rangle \rightarrow |\downarrow'\rangle$ and $|\uparrow\rangle \rightarrow |\uparrow'\rangle$ with respective resonant frequencies ω_\downarrow and $\omega_\uparrow = \omega_\downarrow + \Delta$ can link these states with horizontal polarization, namely, $|H\rangle$, but the two cross transitions corresponding to spin-flipping states are dipole forbidden and thus they are neglected [49]. Here, Δ represents the energy difference between the states $|\downarrow\rangle$ and $|\uparrow\rangle$ caused by the applied magnetic field.

Assuming that an photon in polarized state $|H\rangle$ with frequency ω incorporates into the SiV^- -nanocavity system, where its photonic frequency ω is near resonance with the nanocavity one ω_c , i.e., $\omega \simeq \omega_c$, resulting in the dipole-allowed transition $|\downarrow\rangle \rightarrow |\downarrow'\rangle$ due to destructive interference, but extremely detuned from the other one $|\uparrow\rangle \rightarrow |\uparrow'\rangle$. As a result, when the SiV^- center is initialized to various ground states $|\downarrow\rangle$ and $|\uparrow\rangle$ and is coupled strongly to the nanocavity, the dipole-allowed scattering are different. Moreover, the dynamic equations of motion for the dipole lower operator $\hat{\sigma}_-$ of the SiV^- center and the annihilation operator \hat{a} of the cavity filed in conjunction with the standard input-output relation [51, 52] can be expressed as

$$\begin{aligned} \frac{d\hat{a}}{dt} &= -[i(\omega_c - \omega) + \frac{\kappa}{2}]\hat{a} - g\hat{\sigma}_- - \sqrt{\kappa}\hat{a}_{in} + \hat{N}, \\ \frac{d\hat{\sigma}_-}{dt} &= -[i(\omega_d - \omega) + \frac{\gamma}{2}]\hat{\sigma}_- - g\hat{\sigma}_z\hat{a} + \hat{N}', \\ \hat{a}_{out} &= \hat{a}_{in} + \sqrt{\kappa}\hat{a}. \end{aligned} \quad (1)$$

where $\omega_d(d=\downarrow, \uparrow)$ is the dipole-allowed transition frequency, and κ and γ signify the decay rates of the cavity field and the excited states of the SiV^- center. g represents the coupling ratio between the nanocavity filed and the SiV^- center. The noise operators \hat{N} and \hat{N}' due to the cavity leakage and dipole decay, respectively, are introduced to keep the wanted commutation relations. \hat{a}_{in} and \hat{a}_{out} represent the operators associated with the input and output vacuum fields, respectively. Additionally, $\hat{\sigma}_z$ serves as the population operator for the input photon.

With weak excitation limitation ($\langle \hat{\sigma}_z \rangle = -1$), the reflection coefficient, labeled as $r_s(\omega)$, when an photon enter and interact with the one-sided nanocavity-SiV⁻ system can be accurately expressed as [53]

$$r_d(\omega) = 1 - \frac{2(1 + i\Delta_d)}{C + (1 + i\Delta_d)(1 + i\Delta_c)}, \quad (2)$$

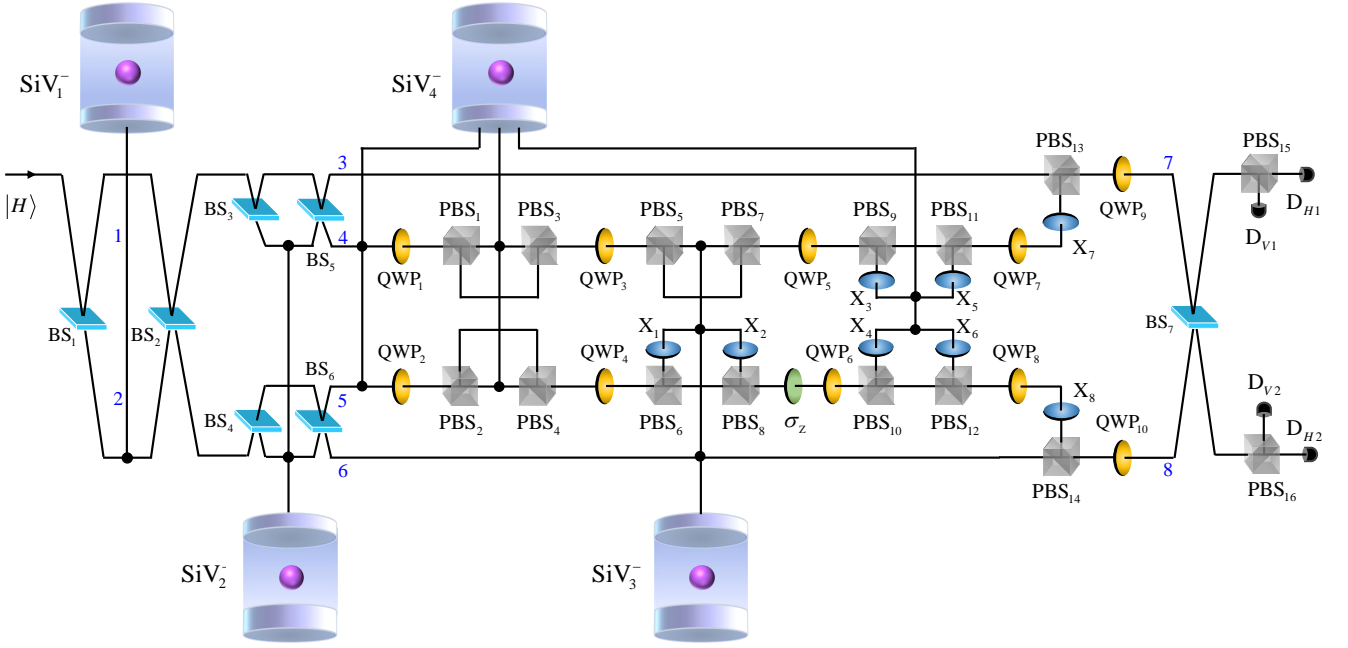


FIG. 2. Schematic diagram of the 2-qudit 4×4 -dimensional CNOT gate for SiV^- centers. The beam splitter ($\text{BS}_n, n = 1, 2, \dots, 7$) completes path transformation between down (d) and up (u) ones, i.e., $N_u \rightarrow (N_u + N_d)/\sqrt{2}$ and $N_d \rightarrow (N_u - N_d)/\sqrt{2}, N \in \{H, V\}$. The polarized beam splitter ($\text{PBS}_i, i = 1, 2, \dots, 16$) transmits (reflects) $|H\rangle$ -($|V\rangle$)-polarized component of one photon. The $X_j (j = 1, 2, \dots, 4)$ fulfills the bit-flip operation $|H\rangle \leftrightarrow |V\rangle$. The quarter-wave plate ($\text{QWP}_k, k = 1, 2, \dots, 10$) fulfills the Hadamard operation. σ_z completes the phase-flip operation $\sigma_z = -|H\rangle\langle H| - |V\rangle\langle V|$. The $\text{SiV}_m^- (m = 1, 2, \dots, 4)$ represents the SiV spin. The single photon detector ($\text{D}_{H1}, \text{D}_{V1}, \text{D}_{H2}$, or D_{V2}) can be used to detect the auxiliary photon.

the subscript $d = \uparrow (\downarrow)$ of the reflection coefficient $r_d(\omega)$ indicates the interaction of the polarized photon with the cavity- SiV^- system. $C = 4g^2/\kappa\gamma$ represents the cooperativity. $\Delta_d = 2(\omega_d - \omega)/\gamma$ and $\Delta_c = 2(\omega_c - \omega)/\kappa$ denote the effective detunings of the dipole-transition and cavity-mode frequencies to be aimed at the input-field frequency ω . Consequently, the input-output relations of the H -polarized photon interacting with one-sided nanocavity- SiV^- -center system can be obtained as $|H\rangle|\downarrow\rangle \rightarrow r_\downarrow(\omega)|H\rangle|\downarrow\rangle$ and $|H\rangle|\uparrow\rangle \rightarrow r_\uparrow(\omega)|H\rangle|\uparrow\rangle$. For $\Delta_c = \Delta_\downarrow = 0$ and $\Delta_\uparrow \gg C \gg 1$, $r_\downarrow = 1$ and $r_\uparrow = -1$ for the SiV^- center in the various ground states $|\downarrow\rangle$ and $|\uparrow\rangle$ for the H -polarized photon can be obtained. In essence, the reflection coefficient $r_d(\omega)$ is governed by the spin state of the SiV^- center [54].

III. A 2-QUDIT 4×4 -DIMENSIONAL CNOT GATE

Now we set up the deterministic 2-qudit 4×4 -dimensional CNOT gate for a four- SiV^- system with a auxiliary photon in Figure 2. Here, we encode spin states $|\downarrow\downarrow\rangle_{12}, |\downarrow\uparrow\rangle_{12}, |\uparrow\downarrow\rangle_{12}$, and $|\uparrow\uparrow\rangle_{12}$ of two SiV_1^- and SiV_2^- centers as control qudits $|0\rangle_c, |1\rangle_c, |2\rangle_c$, and $|3\rangle_c$, respectively, and the other ones $|\downarrow\downarrow\rangle_{34}, |\downarrow\uparrow\rangle_{34}, |\uparrow\downarrow\rangle_{34}$, and $|\uparrow\uparrow\rangle_{34}$ of SiV_3^- and SiV_4^- centers as the target qudits $|0\rangle_t, |1\rangle_t, |2\rangle_t$, and $|3\rangle_t$, respectively. The 2-qudit 4×4 -dimensional CNOT gate makes the target qudit in state $|t\rangle$ to become $|(c+t)\%4\rangle$ when the control qudit is in state $|c\rangle$, as the following transformation [19]:

$$\begin{aligned}
 |0_c, 0_t\rangle &\rightarrow |0_c, 0_t\rangle, & |0_c, 1_t\rangle &\rightarrow |0_c, 1_t\rangle, & |0_c, 2_t\rangle &\rightarrow |0_c, 2_t\rangle, & |0_c, 3_t\rangle &\rightarrow |0_c, 3_t\rangle, \\
 |1_c, 0_t\rangle &\rightarrow |1_c, 1_t\rangle, & |1_c, 1_t\rangle &\rightarrow |1_c, 2_t\rangle, & |1_c, 2_t\rangle &\rightarrow |1_c, 3_t\rangle, & |1_c, 3_t\rangle &\rightarrow |1_c, 0_t\rangle, \\
 |2_c, 0_t\rangle &\rightarrow |2_c, 2_t\rangle, & |2_c, 1_t\rangle &\rightarrow |2_c, 3_t\rangle, & |2_c, 2_t\rangle &\rightarrow |2_c, 0_t\rangle, & |2_c, 3_t\rangle &\rightarrow |2_c, 1_t\rangle, \\
 |3_c, 0_t\rangle &\rightarrow |3_c, 3_t\rangle, & |3_c, 1_t\rangle &\rightarrow |3_c, 0_t\rangle, & |3_c, 2_t\rangle &\rightarrow |3_c, 1_t\rangle, & |3_c, 3_t\rangle &\rightarrow |3_c, 2_t\rangle.
 \end{aligned} \tag{3}$$

Suppose that the control two spins of two SiV_1^- and SiV_2^- centers is originally prepared in state $|\psi\rangle_c = \alpha_1|3\rangle_c + \alpha_2|2\rangle_c + \alpha_3|1\rangle_c + \alpha_4|0\rangle_c$ and the control two spins of two SiV_3^- and SiV_4^- centers is originally prepared in state $|\psi\rangle_t = \gamma_1|3\rangle_t + \gamma_2|2\rangle_t + \gamma_3|1\rangle_t + \gamma_4|0\rangle_t$, respectively. Here, $|B_1|^2 + |B_2|^2 + |B_3|^2 + |B_4|^2 = 1$, ($B = \alpha, \gamma$). The ancillary single photon is originally prepared in state $|H\rangle$. Thus, the state of the whole system involving the single photon and four SiV^- centers is $|\Psi\rangle_0 = |H\rangle \otimes |\psi\rangle_c \otimes |\psi\rangle_t$.

Firstly, the single photon experiences some operations as follows: $\text{BS}_1 \rightarrow \text{SiV}_1^-$ -cavity system $\rightarrow \text{BS}_2 \rightarrow \text{BS}_3, \text{BS}_4 \rightarrow \text{SiV}_2^-$ -cavity system $\rightarrow \text{BS}_5, \text{BS}_6$. Here, the optical element beam splitter ($\text{BS}_n, n = 1, 2, \dots, 6$) completes path transformations between down (d) and up (u) ones, i.e., $H_u \rightarrow (H_u + H_d)/\sqrt{2}$ and $H_d \rightarrow (H_u - H_d)/\sqrt{2}$. After these operations, the state $|\Psi\rangle_0$ of the whole system is evolved into

$$|\Psi\rangle_1 = (\alpha_1|H\rangle^5|3\rangle_c + \alpha_2|H\rangle^6|2\rangle_c + \alpha_3|H\rangle^4|1\rangle_c + \alpha_4|H\rangle^3|0\rangle_c) \otimes (\gamma_1|3\rangle + \gamma_2|2\rangle + \gamma_3|1\rangle + \gamma_4|0\rangle)_t. \quad (4)$$

Secondly, before and after the auxiliary photon in path 4 (path 5) interacts with SiV_4^- -cavity system, the Hadamard operation H_e aiming at the spin of the SiV_4^- by taking advantage of a $\pi/2$ microwave pulse completes the transformations $|+\rangle \rightarrow \frac{1}{\sqrt{2}}(|+\rangle + |-\rangle)$ and $|-\rangle \rightarrow \frac{1}{\sqrt{2}}(|+\rangle - |-\rangle)$. After the first interaction between the auxiliary photon and the SiV_4^- -cavity system, the state $|\Psi\rangle_1$ of the whole system is changed into

$$|\Psi\rangle_2 = \alpha_1|H\rangle^5|3\rangle_c \otimes (\gamma_1|2\rangle + \gamma_2|3\rangle + \gamma_3|0\rangle + \gamma_4|1\rangle)_t + \alpha_2|H\rangle^6|2\rangle_c \otimes (\gamma_1|3\rangle + \gamma_2|2\rangle + \gamma_3|1\rangle + \gamma_4|0\rangle)_t + \alpha_3|H\rangle^4|1\rangle_c \otimes (\gamma_1|2\rangle + \gamma_2|3\rangle + \gamma_3|0\rangle + \gamma_4|1\rangle)_t + \alpha_4|H\rangle^3|0\rangle_c \otimes (\gamma_1|3\rangle + \gamma_2|2\rangle + \gamma_3|1\rangle + \gamma_4|0\rangle)_t. \quad (5)$$

Thirdly, the photon on path 4 (path 5) experiences following operations: $\text{QWP}_1(\text{QWP}_2) \rightarrow \text{PBS}_1(\text{PBS}_2) \rightarrow \text{SiV}_4^-$ -cavity system $\rightarrow \text{PBS}_3(\text{PBS}_4) \rightarrow \text{QWP}_3(\text{QWP}_4)$, where the polarized beam splitter ($\text{PBS}_i, i = 1, 2, \dots, 4$) transmits (reflects) $|H\rangle$ -($|V\rangle$)-polarized component of the photon and meanwhile the optical element quarter-wave plate $\text{QWP}_k(k = 1, 2, \dots, 4)$ is to perform the Hadamard operation on the auxiliary photon, i.e., $|H\rangle \rightarrow \frac{1}{\sqrt{2}}(|H\rangle + |V\rangle)$ and $|V\rangle \rightarrow \frac{1}{\sqrt{2}}(|H\rangle - |V\rangle)$. After the second interaction between the auxiliary photon and the SiV_4^- -cavity system, the state $|\Psi\rangle_2$ of the whole system is changed into

$$|\Psi\rangle_3 = \alpha_1|H\rangle^5|3\rangle_c \otimes (\gamma_1|2\rangle + \gamma_3|0\rangle)_t - \alpha_1|V\rangle^5|3\rangle_c \otimes (\gamma_2|3\rangle + \gamma_4|1\rangle)_t + \alpha_2|H\rangle^6|2\rangle_c \otimes (\gamma_1|3\rangle + \gamma_2|2\rangle + \gamma_3|1\rangle + \gamma_4|0\rangle)_t + \alpha_3|H\rangle^4|1\rangle_c \otimes (\gamma_1|2\rangle + \gamma_3|0\rangle)_t - \alpha_3|V\rangle^4|1\rangle_c \otimes (\gamma_2|3\rangle + \gamma_4|1\rangle)_t + \alpha_4|H\rangle^3|0\rangle_c \otimes (\gamma_1|3\rangle + \gamma_2|2\rangle + \gamma_3|1\rangle + \gamma_4|0\rangle)_t. \quad (6)$$

Fourthly, the photon on path 4 (path 5) experiences following operations: $\text{PBS}_5(\text{PBS}_6, X_1) \rightarrow \text{SiV}_3^-$ -cavity system $\rightarrow \text{PBS}_7(X_2, \text{PBS}_8, \sigma_z)$, meanwhile, the photon on path 6 also interacts with SiV_3^- -cavity system. Here, the optical element $X_j(j = 1, 2, \dots, 4)$ is a half-wave plate fixed at 45° to fulfill a bit-flip operation $|H\rangle \leftrightarrow |V\rangle$ and σ_z completes the phase-flip operation $\sigma_z = -|H\rangle\langle H| - |V\rangle\langle V|$. Notably, before and after the photon experiences these operations, H^e should be acted on the spin of SiV_3^- center, resulting in

$$|\Psi\rangle_4 = \alpha_1|H\rangle^5|3\rangle_c \otimes (\gamma_1|2\rangle + \gamma_3|0\rangle)_t + \alpha_1|V\rangle^5|3\rangle_c \otimes (\gamma_2|1\rangle + \gamma_4|3\rangle)_t + \alpha_2|H\rangle^6|2\rangle_c \otimes (\gamma_1|1\rangle + \gamma_2|0\rangle + \gamma_3|3\rangle + \gamma_4|2\rangle)_t + \alpha_3|H\rangle^4|1\rangle_c \otimes (\gamma_1|0\rangle + \gamma_3|2\rangle)_t - \alpha_3|V\rangle^4|1\rangle_c \otimes (\gamma_2|3\rangle + \gamma_4|1\rangle)_t + \alpha_4|H\rangle^3|0\rangle_c \otimes (\gamma_1|3\rangle + \gamma_2|2\rangle + \gamma_3|1\rangle + \gamma_4|0\rangle)_t. \quad (7)$$

Fifthly, the photon on path 4 (path 5) experiences following operations: $\text{QWP}_5(\text{QWP}_6) \rightarrow \text{PBS}_9(\text{PBS}_{10}) \rightarrow X_3(X_4) \rightarrow \text{SiV}_4^-$ -cavity system $\rightarrow X_5(X_6) \rightarrow \text{PBS}_{11}(\text{PBS}_{12}) \rightarrow \text{QWP}_7(\text{QWP}_8) \rightarrow X_7(X_8) \rightarrow \text{PBS}_{13}(\text{PBS}_{14})$ mixed at path 7 (8). After the third interaction between the auxiliary photon and the SiV_4^- -cavity system, leading to

$$|\Psi\rangle_5 = \alpha_1|V\rangle^8|3\rangle_c \otimes (\gamma_1|2\rangle + \gamma_2|1\rangle + \gamma_3|0\rangle + \gamma_4|3\rangle)_t + \alpha_2|H\rangle^8|2\rangle_c \otimes (\gamma_1|1\rangle + \gamma_2|0\rangle + \gamma_3|3\rangle + \gamma_4|2\rangle)_t + \alpha_3|V\rangle^7|1\rangle_c \otimes (\gamma_1|0\rangle + \gamma_2|3\rangle + \gamma_3|2\rangle + \gamma_4|1\rangle)_t + \alpha_4|H\rangle^7|0\rangle_c \otimes (\gamma_1|3\rangle + \gamma_2|2\rangle + \gamma_3|1\rangle + \gamma_4|0\rangle)_t. \quad (8)$$

Finally, the photon on path 7 (path 8) experiences following operations: $\text{QWP}_9(\text{QWP}_{10}) \rightarrow \text{BS}_7 \rightarrow \text{PBS}_{15}(\text{PBS}_{16})$, resulting in

$$|\Psi\rangle_6 = |D_{H1}\rangle \otimes [\alpha_1|3\rangle_c \otimes (\gamma_1|2\rangle + \gamma_2|1\rangle + \gamma_3|0\rangle + \gamma_4|3\rangle)_t + \alpha_2|2\rangle_c \otimes (\gamma_1|1\rangle + \gamma_2|0\rangle + \gamma_3|3\rangle + \gamma_4|2\rangle)_t + \alpha_3|1\rangle_c \otimes (\gamma_1|0\rangle + \gamma_2|3\rangle + \gamma_3|2\rangle + \gamma_4|1\rangle)_t]$$

$$\begin{aligned}
& +\alpha_4|0\rangle_c \otimes (\gamma_1|3\rangle + \gamma_2|2\rangle + \gamma_3|1\rangle + \gamma_4|0\rangle)_t \\
& +|D_{V1}\rangle \otimes [-\alpha_1|3\rangle_c \otimes (\gamma_1|2\rangle + \gamma_2|1\rangle + \gamma_3|0\rangle + \gamma_4|3\rangle)_t \\
& -\alpha_2|2\rangle_c \otimes (\gamma_1|1\rangle + \gamma_2|0\rangle + \gamma_3|3\rangle + \gamma_4|2\rangle)_t \\
& +\alpha_3|1\rangle_c \otimes (\gamma_1|0\rangle + \gamma_2|3\rangle + \gamma_3|2\rangle + \gamma_4|1\rangle)_t \\
& +\alpha_4|0\rangle_c \otimes (\gamma_1|3\rangle + \gamma_2|2\rangle + \gamma_3|1\rangle + \gamma_4|0\rangle)_t \\
& +|D_{H2}\rangle \otimes [-\alpha_1|3\rangle_c \otimes (\gamma_1|2\rangle + \gamma_2|1\rangle + \gamma_3|0\rangle + \gamma_4|3\rangle)_t \\
& +\alpha_2|2\rangle_c \otimes (\gamma_1|1\rangle + \gamma_2|0\rangle + \gamma_3|3\rangle + \gamma_4|2\rangle)_t \\
& -\alpha_3|1\rangle_c \otimes (\gamma_1|0\rangle + \gamma_2|3\rangle + \gamma_3|2\rangle + \gamma_4|1\rangle)_t \\
& +\alpha_4|0\rangle_c \otimes (\gamma_1|3\rangle + \gamma_2|2\rangle + \gamma_3|1\rangle + \gamma_4|0\rangle)_t \\
& +|D_{V2}\rangle \otimes [\alpha_1|3\rangle_c \otimes (\gamma_1|2\rangle + \gamma_2|1\rangle + \gamma_3|0\rangle + \gamma_4|3\rangle)_t \\
& -\alpha_2|2\rangle_c \otimes (\gamma_1|1\rangle + \gamma_2|0\rangle + \gamma_3|3\rangle + \gamma_4|2\rangle)_t \\
& -\alpha_3|1\rangle_c \otimes (\gamma_1|0\rangle + \gamma_2|3\rangle + \gamma_3|2\rangle + \gamma_4|1\rangle)_t \\
& +\alpha_4|0\rangle_c \otimes (\gamma_1|3\rangle + \gamma_2|2\rangle + \gamma_3|1\rangle + \gamma_4|0\rangle)_t].
\end{aligned} \tag{9}$$

In evidence, if the detector D_{H1} responses, the standard 2-qudit 4×4 -dimensional CNOT gate acting on four SiV^- centers can be established successfully, i.e.,

$$\begin{aligned}
|\Phi_0\rangle &= \alpha_1|3\rangle_c \otimes (\gamma_1|2\rangle + \gamma_2|1\rangle + \gamma_3|0\rangle + \gamma_4|3\rangle)_t \\
& +\alpha_2|2\rangle_c \otimes (\gamma_1|1\rangle + \gamma_2|0\rangle + \gamma_3|3\rangle + \gamma_4|2\rangle)_t \\
& +\alpha_3|1\rangle_c \otimes (\gamma_1|0\rangle + \gamma_2|3\rangle + \gamma_3|2\rangle + \gamma_4|1\rangle)_t \\
& +\alpha_4|0\rangle_c \otimes (\gamma_1|3\rangle + \gamma_2|2\rangle + \gamma_3|1\rangle + \gamma_4|0\rangle)_t.
\end{aligned} \tag{10}$$

Otherwise, if the detectors D_{V1} (or D_{H2} , D_{V2}) responses, the nonstandard 2-qudit CNOT gate can be obtained, i.e.,

$$\begin{aligned}
|\Phi_1\rangle &= -\alpha_1|3\rangle_c \otimes (\gamma_1|2\rangle + \gamma_2|1\rangle + \gamma_3|0\rangle + \gamma_4|3\rangle)_t \\
& -\alpha_2|2\rangle_c \otimes (\gamma_1|1\rangle + \gamma_2|0\rangle + \gamma_3|3\rangle + \gamma_4|2\rangle)_t \\
& +\alpha_3|1\rangle_c \otimes (\gamma_1|0\rangle + \gamma_2|3\rangle + \gamma_3|2\rangle + \gamma_4|1\rangle)_t \\
& +\alpha_4|0\rangle_c \otimes (\gamma_1|3\rangle + \gamma_2|2\rangle + \gamma_3|1\rangle + \gamma_4|0\rangle)_t, \\
|\Phi_2\rangle &= -\alpha_1|3\rangle_c \otimes (\gamma_1|2\rangle + \gamma_2|1\rangle + \gamma_3|0\rangle + \gamma_4|3\rangle)_t \\
& +\alpha_2|2\rangle_c \otimes (\gamma_1|1\rangle + \gamma_2|0\rangle + \gamma_3|3\rangle + \gamma_4|2\rangle)_t \\
& -\alpha_3|1\rangle_c \otimes (\gamma_1|0\rangle + \gamma_2|3\rangle + \gamma_3|2\rangle + \gamma_4|1\rangle)_t \\
& +\alpha_4|0\rangle_c \otimes (\gamma_1|3\rangle + \gamma_2|2\rangle + \gamma_3|1\rangle + \gamma_4|0\rangle)_t, \\
|\Phi_3\rangle &= \alpha_1|3\rangle_c \otimes (\gamma_1|2\rangle + \gamma_2|1\rangle + \gamma_3|0\rangle + \gamma_4|3\rangle)_t \\
& -\alpha_2|2\rangle_c \otimes (\gamma_1|1\rangle + \gamma_2|0\rangle + \gamma_3|3\rangle + \gamma_4|2\rangle)_t \\
& -\alpha_3|1\rangle_c \otimes (\gamma_1|0\rangle + \gamma_2|3\rangle + \gamma_3|2\rangle + \gamma_4|1\rangle)_t \\
& +\alpha_4|0\rangle_c \otimes (\gamma_1|3\rangle + \gamma_2|2\rangle + \gamma_3|1\rangle + \gamma_4|0\rangle)_t.
\end{aligned} \tag{11}$$

Apparently, the corresponding single-qubit feed-forward operation $\sigma_z = |\downarrow\rangle\langle\downarrow| - |\uparrow\rangle\langle\uparrow|$ with a π microwave pulse is performed on SiV_1^- (or SiV_2^-) center, the state $|\Phi_1\rangle$ (or $|\Phi_2\rangle$) can be changed into the one in Eq. (10). In detail, for the case that D_{V1} is triggered, a σ_z is acted on the SiV_2^- center; for the case that D_{H2} is triggered, a $-\sigma_z$ is acted on the SiV_1^- center. Besides, for the case that D_{V2} is triggered, another auxiliary H -polarization photon interact with the SiV_1^- and SiV_2^- again, we can change the state $|\Phi_3\rangle$ to the one $|\Phi_0\rangle$ in Eq. (10). As a consequence, we get the deterministic 2-qudit CNOT gate with unity success probability in principle on account of the reflection-selective rule of the ancillary single photon.

IV. DISCUSSION AND CONCLUSION

So far, we have set up definitely a 2-qudit 4×4 -dimensional CNOT gate for the four- SiV^- system by virtue of perfect optical transitions and efficacious interaction between the auxiliary photon and four SiV^- spins, where the auxiliary H -polarization photon carrying an input frequency ω with lower decoherence and shorter operation time interacts each SiV^- center in two ground states $|\downarrow\rangle$ and $|\uparrow\rangle$ and derive various phases 0 and π from the reflection

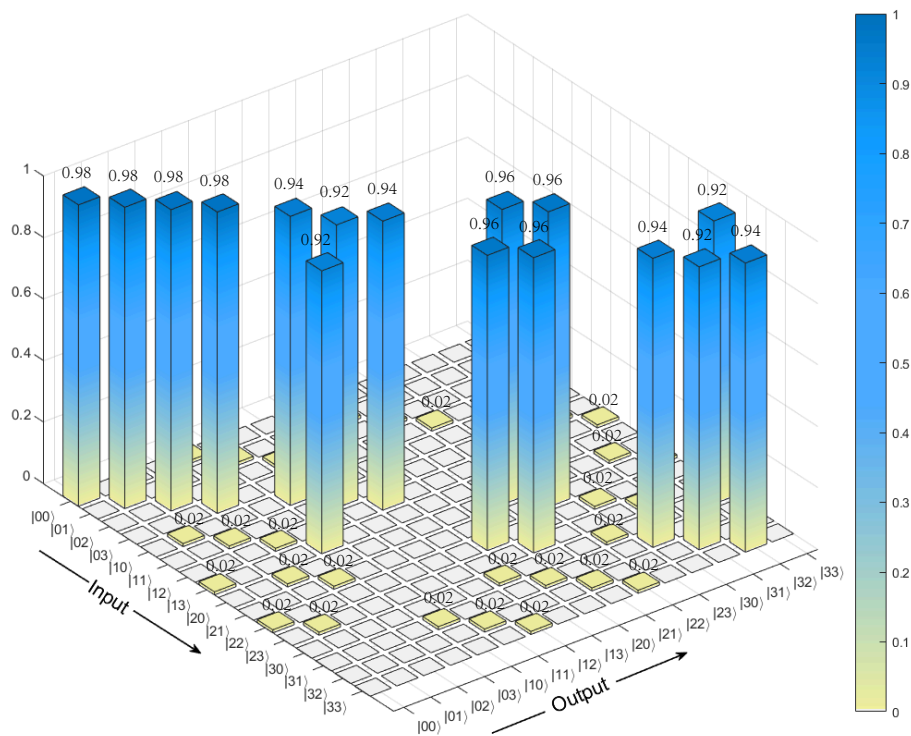


FIG. 3. The probability of all computational basis states occurring after applying the 2-qudit CNOT gate to each of the computational basis states for four SiV^- centers vs the 4×4 -dimensional set of input states with the condition $r_\downarrow = -r_\uparrow = 0.98$ in Ref. [54].

coefficients $r_\downarrow(\omega) = +1$ and $r_\uparrow(\omega) = -1$, respectively. Suppose that the detection efficiency of the detector D_{H1} (or D_{V1} , D_{H2} , D_{V2}) is unity, the efficiency of our protocol is mainly impacted from the interacting loss, when the linear optical elements, i.e., PBSs and BSs are ideal ignoring the errors. The fidelity F defined in the paper [19] of our 2-qudit CNOT gate shown in Figure 3. (a) approach unity in the 4×4 -dimensional set of input states $\{|00\rangle, |01\rangle, |02\rangle, |03\rangle, |10\rangle, |11\rangle, |12\rangle, |13\rangle, |20\rangle, |21\rangle, |22\rangle, |23\rangle, |30\rangle, |31\rangle, |32\rangle, \text{ and } |33\rangle\}$.

As external fields and local strain are variable, dissimilar detunings of optical transitions aiming at four SiV^- centers, it is essential to compensate energetically these detunings by adjusting external fields and and the strain [55–57]. Furthermore, imperfect factors, i.e., a limited detuning Δ_\uparrow and a finite cooperativity C owing to a tiny coupling g coupling a spin to an optical nanocavity, lead to a nonideal interaction process with the coefficient $r_d(\omega)$ designated in Eq.(2). Especially, both the reflection coefficients r_\downarrow and $-r_\uparrow$ with respect of various ground states equal to 0.98, holding opposite phases and same amplitude in a condition with $C = 100$, $\Delta_\uparrow = 100$, and $\Delta_c = 1$ in Ref. [54]. The Figure 3 shows the probabilities of all computational basis states after applying the four-dimensional CNOT gate to each of the computational basis states, the minimum effective conversion rate is $P = 92.27\%$.

The performance of the 2-qudit 4×4 -dimensional CNOT gate is described by efficiency and fidelity, which are affected by the reflection coefficient. Here, we treat the SiV^- centers as identical ones for convenience. The reflection coefficient is shown in Equation (2), an increase in the effective detunings of cavity-mode frequencies Δ_\uparrow will raises the reflection coefficient $|r_d(\omega)|$ closer to 1, as does decreasing the dipole-transition Δ_\downarrow and cavity-mode frequencies Δ_c . The efficiency of these gates can approach unity when $\Delta_c = \Delta_\downarrow = 0$ and $\Delta_\uparrow \gg C \gg 1$. With parameters $(g, \gamma, \kappa) = 2\pi \times (8.4, 0.1, 28.2)$ GHz in Ref. [50], the cooperativity C can approximately reach 100. Besides, the large optical splitting $\Delta_c - \Delta_\uparrow = -99$ of two effective optical transitions $|\downarrow\rangle \rightarrow |\downarrow'\rangle$ and $|\uparrow\rangle \rightarrow |\uparrow'\rangle$ can be achieved in case of moderate strain 10^{-7} and the magnetic field $B \sim 0.5T$, where the difference of Landé g factors between the ground and excited states is $\delta g = 0.06$ and meanwhile the orbital splitting of two ground states is $\Delta \sim 140$ GHz [49]. And with the reflection coefficient $r_\downarrow = -r_\uparrow = [0.95, 0.96, 0.98, 1]$, the efficiencies $\eta_C = [0.8613, 0.8876, 0.9427, 1]$ shown in Figure 4. (a) and the fidelities $F_C = [0.9971, 0.9981, 0.9995, 1]$ shown in Figure 4. (b) for CNOT gate can be achieved.

Generally speaking, the decoherence of the SiV^- center also reduces the fidelity of the four-dimensional CNOT gate and its influence on the fidelity coming from two aspects, where one is the defective scattering of the auxiliary photon with each SiV^- spin, the other one is the propagation of the auxiliary photon over quantum channels between

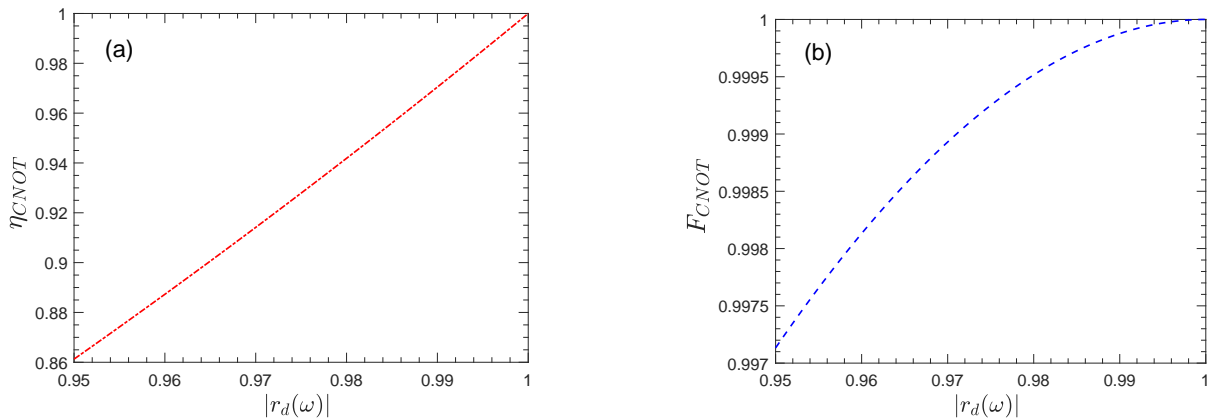


FIG. 4. (a) The efficiency and (b) fidelity versus the reflection coefficient $|r_d(\omega)|$.

neighboring two SiV^- spins. For the former, the spin decoherence falls off the fidelity defined as $[exp(-t_T/T_2^e) + 1]/2$, when each SiV^- spin experiences respective decoherence [58, 59]. Here t_T (\sim microsecond) is the total interaction time in each SiV^- -cavity system and the T_2^e ($> 10ms$) is the electron-spin coherence time of the SiV^- at 100 mK [60]. Therefore, the decoherence of the SiV^- spin decreases the fidelity of the 4×4 -dimensional CNOT gate less than 0.005 during interaction processes in each SiV^- . Besides, the imperfect mode matching between polarized state $|H\rangle$ of the auxiliary photon and the optical transition of the SiV^- result in an error, decreasing the fidelity 10^{-4} of our CNOT gate for an available mode-matching efficiency of 0.99 [61].

In summary, we have shown that it is possible to implement a computation-enhanced 2-qudit CNOT gate for four SiV^- spins with a auxiliary photon, in which the control qudits encode the information on the spin states of SiV_1^- and SiV_2^- centers, and the other ones of SiV_3^- and SiV_4^- centers as the target qudits. The ancillary photon in state $|H\rangle$ is used to interact with four stationary SiV^- spins embedded in four independent single-sided optical nanocavities and link them together. Moreover, the CNOT gate works in a deterministic way with perfect optical transitions and efficacious interaction by performing the relational feed-forward operations corresponding to the different outcomes of the single-photon detectors to be aimed at the ancillary photon. Further, it can be potentially generalized to other solid-state quantum system, namely, quantum dots, nuclear magnetic resonance, atoms, and nitrogen-vacancy centers. The fidelity F of the 2-qudit CNOT gate for four SiV^- centers have satisfactory performances by exploiting existing technological conditions. In contrast to pre-existing 2×2 -dimensional CNOT gates CNOT gates [35–40], the 2-qudit 4×4 -dimensional CNOT gate operating on solid-state quantum systems provide not only the scalability to realize more complex quantum operations given in Eq. (10), but also the experimental flexibility to enhance practically the speed of quantum computing.

ACKNOWLEDGMENTS

This work was supported in part by the Natural Science Foundation of China under Contract 61901420; in part by Fundamental Research Program of Shanxi Province under Contract 20230302121116.

DISCLOSURES

The authors declare no conflicts of interest.

DATA AVAILABILITY STATEMENT

Data underlying the results presented in this paper are not publicly available at this time but may be obtained from the authors upon reasonable request.

-
- [1] D. D. Awschalom, R. Hanson, J. Wrachtrup, and B. B. Zhou, Quantum technologies with optically interfaced solid-state spins, *Nat. Photonics* **12**, 516 (2018).
 - [2] Y.-L. Liu, M.-W. Wang, C.-Y. Bai, and T.-J. Wang, Asymmetrical bell state analysis for photon-atoms hybrid system, *Sci. China Phys. Mech. Astron* **62**, 120311 (2019).
 - [3] W.-T. He, C.-W. Lu, Y.-X. Yao, H.-Y. Zhu, and Q. Ai, Criticality-based quantum metrology in the presence of decoherence, *Front. Phys.* **18**, 31304 (2023).
 - [4] J. Li, Z. Xie, Y. Li, Y. Liang, Z. Li, and T. Li, Heralded entanglement between error-protected logical qubits for fault-tolerant distributed quantum computing, *Sci. China Phys. Mech.* **67**, 220311 (2024).
 - [5] V. Lahtinen and J. K. Pachos, A Short Introduction to Topological Quantum Computation, *SciPost Phys.* **3**, 021 (2017).
 - [6] G. Z. Song, J. L. Guo, Q. Liu, H. R. Wei, and G. L. Long, Heralded quantum gates for hybrid systems via waveguide-mediated photon scattering, *Phys. Rev. A* **104**, 012608 (2021).
 - [7] W.-Q. Liu and H.-R. Wei, Linear optical universal quantum gates with higher success probabilities, *Adv. Quantum Technol.* **6**, 2300009 (2023).
 - [8] X.-J. Zhou, W.-Q. Liu, H.-R. Wei, Y.-B. Zheng, and F.-F. Du, Deterministic and complete hyperentangled bell states analysis assisted by frequency and time interval degrees of freedom, *Front. Phys.* **17**, 41502 (2022).
 - [9] S. P. Kelly, U. Poschinger, F. Schmidt-Kaler, M. P. A. Fisher, and J. Marino, Coherence requirements for quantum communication from hybrid circuit dynamics, *SciPost Phys.* **15**, 250 (2023).
 - [10] Y. LIU, G. L. LONG, and Y. SUN, Analytic one-bit and cnot gate constructions of general n-qubit controlled gates, *Int. J. Quantum Inf.* **06**, 447 (2008).
 - [11] G.-L. Jiang, W.-Q. Liu, and H.-R. Wei, Practically enhanced hyperentanglement concentration for polarization-spatial hyperentangled bell states with linear optics and common single-photon detectors, *Phys. Rev. Appl.* **19**, 034044 (2023).
 - [12] P.-S. Yan, L. Zhou, W. Zhong, and Y.-B. Sheng, Measurement-based logical qubit entanglement purification, *Phys. Rev. A* **105**, 062418 (2022).
 - [13] P.-S. Yan, L. Zhou, W. Zhong, and Y.-B. Sheng, Measurement-based entanglement purification for entangled coherent states, *Front. Phys.* **17**, 1 (2022).
 - [14] Z.-D. Ye, D. Pan, Z. Sun, C.-G. Du, L.-G. Yin, and G.-L. Long, Generic security analysis framework for quantum secure direct communication, *Front. Phys.* **16**, 1 (2021).
 - [15] L. Zhou, B.-W. Xu, W. Zhong, and Y.-B. Sheng, Device-independent quantum secure direct communication with single-photon sources, *Phys. Rev. Appl.* **19**, 014036 (2023).
 - [16] Y.-F. Yan, L. Zhou, W. Zhong, and Y.-B. Sheng, Measurement-device-independent quantum key distribution of multiple degrees of freedom of a single photon, *Front. Phys.* **16**, 1 (2021).
 - [17] L. Y. He, T.-J. Wang, and C. Wang, Construction of high-dimensional universal quantum logic gates using a λ system coupled with a whispering-gallery-mode microresonator, *Opt. Express* **24**, 15429 (2016).
 - [18] B. P. Lanyon, M. Barbieri, M. P. Almeida, T. Jennewein, T. C. Ralph, K. J. Resch, G. J. Pryde, J. L. O'Brien, A. Gilchrist, and A. G. White, Simplifying quantum logic using higher-dimensional hilbert spaces, *Nat. Phys.* **5**, 134 (2009).
 - [19] X. Gao, M. Erhard, A. Zeilinger, and M. Krenn, Computer-inspired concept for high-dimensional multipartite quantum gates, *Phys. Rev. Lett.* **125**, 050501 (2020).
 - [20] A. Babazadeh, M. Erhard, F. Wang, M. Malik, R. Nouroozi, M. Krenn, and A. Zeilinger, High-dimensional single-photon quantum gates: Concepts and experiments, *Phys. Rev. Lett.* **119**, 180510 (2017).
 - [21] N.-F. Gong, T.-J. Wang, and S. Ghose, Control power of a high-dimensional controlled nonlocal quantum computation, *Phys. Rev. A* **103**, 052601 (2021).
 - [22] W. Q. Liu and H. R. Wei, Optimal synthesis of the fredkin gate in a multilevel system, *New J. Phys.* **22**, 063026 (2020).
 - [23] W. Q. Liu, H. R. Wei, and L. C. Kwek, Low-cost fredkin gate with auxiliary space, *Phys. Rev. Appl.* **14**, 054057 (2020).
 - [24] E. Knill, R. Laflamme, and G. J. Milburn, A scheme for efficient quantum computation with linear optics, *nature* **409**, 46 (2001).
 - [25] J. L. O'Brien, G. J. Pryde, A. G. White, T. C. Ralph, and D. Branning, Demonstration of an all-optical quantum controlled-not gate, *Nature* **426**, 264 (2003).
 - [26] G.-L. Jiang, J.-B. Yuan, W.-Q. Liu, and H.-R. Wei, Efficient and deterministic high-dimensional controlled-swap gates on hybrid linear optical systems with high fidelity, *Phys. Rev. Appl.* **21**, 014001 (2024).
 - [27] T. Yamamoto, Y. A. Pashkin, O. Astafiev, Y. Nakamura, and J. S. Tsai, Demonstration of conditional gate operation using superconducting charge qubits, *Nature* **425**, 941 (2003).
 - [28] J. M. Chow, J. M. Gambetta, A. D. Córcoles, S. T. Merkel, J. A. Smolin, C. Rigetti, S. Poletto, G. A. Keefe, M. B. Rothwell, J. R. Rozen, M. B. Ketchen, and M. Steffen, Universal quantum gate set approaching fault-tolerant thresholds with superconducting qubits, *Phys. Rev. Lett.* **109**, 060501 (2012).

- [29] G. Feng, G. Xu, and G. Long, Experimental realization of nonadiabatic holonomic quantum computation, *Phys. Rev. Lett.* **110**, 190501 (2013).
- [30] T. Xin, J. S. Pedernales, E. Solano, and G.-L. Long, Entanglement measures in embedding quantum simulators with nuclear spins, *Phys. Rev. A* **97**, 022322 (2018).
- [31] L. M. Duan and H. Kimble, Scalable photonic quantum computation through cavity-assisted interactions, *Phys. Rev. Lett.* **92**, 127902 (2004).
- [32] L. Isenhower, E. Urban, X. Zhang, A. Gill, T. Henage, T. A. Johnson, T. Walker, and M. Saffman, Demonstration of a neutral atom controlled-not quantum gate, *Phys. Rev. Lett.* **104**, 010503 (2010).
- [33] A. Reiserer, N. Kalb, G. Rempe, and S. Ritter, A quantum gate between a flying optical photon and a single trapped atom, *Nature* **508**, 237 (2014).
- [34] B. Hacker, S. Welte, G. Rempe, and S. Ritter, A photon-photon quantum gate based on a single atom in an optical resonator, *Nature* **536**, 193 (2016).
- [35] T.-J. Wang and C. Wang, Universal hybrid three-qubit quantum gates assisted by a nitrogen-vacancy center coupled with a whispering-gallery-mode microresonator, *Phys. Rev. A* **90**, 052310 (2014).
- [36] C. Wang, Y. Zhang, R. Z. Jiao, and G. S. Jin, Universal quantum controlled phase gate on photonic qubits based on nitrogen vacancy centers and microcavity resonators, *Opt. Express* **21**, 19252 (2013).
- [37] H. R. Wei and F. G. Deng, Compact quantum gates on electron-spin qubits assisted by diamond nitrogen-vacancy centers inside cavities, *Phys. Rev. A* **88**, 042323 (2013).
- [38] X. Q. Li, Y. W. Wu, D. C. Steel, D. Gammon, T. Stievater, D. Katzer, D. Park, C. Piermarocchi, and L. Sham, An all-optical quantum gate in a semiconductor quantum dot, *Science* **301**, 809 (2003).
- [39] C. Bonato, F. Haupt, S. S. R. Oemrawsingh, J. Gudat, D. Ding, M. P. van Exter, and D. Bouwmeester, Cnot and bell-state analysis in the weak-coupling cavity qed regime, *Phys. Rev. Lett.* **104**, 160503 (2010).
- [40] H. R. Wei and F. G. Deng, Universal quantum gates for hybrid systems assisted by quantum dots inside double-sided optical microcavities, *Phys. Rev. A* **87**, 022305 (2013).
- [41] M. Gomanko, E. J. de Jong, Y. Jiang, S. G. Schellingerhout, E. P. A. M. Bakkers, and S. M. Frolov, Spin and Orbital Spectroscopy in the Absence of Coulomb Blockade in Lead Telluride Nanowire Quantum Dots, *SciPost Phys.* **13**, 089 (2022).
- [42] Y.-F. Qiao, H.-Z. Li, X.-L. Dong, J.-Q. Chen, Y. Zhou, and P.-B. Li, Phononic-waveguide-assisted steady-state entanglement of silicon-vacancy centers, *Phys. Rev. A* **101**, 042313 (2020).
- [43] B. Pingault, J. N. Becker, C. H. H. Schulte, C. Arend, C. Hepp, T. Godde, A. I. Tartakovskii, M. Markham, C. Becher, and M. Atatüre, All-optical formation of coherent dark states of silicon-vacancy spins in diamond, *Phys. Rev. Lett.* **113**, 263601 (2014).
- [44] J. N. Becker, J. Görlitz, C. Arend, M. Markham, and C. Becher, Ultrafast all-optical coherent control of single silicon vacancy colour centres in diamond, *Nature Communications* **7**, 13512 (2016).
- [45] C. Weinzetl, J. Görlitz, J. N. Becker, I. A. Walmsley, E. Poem, J. Nunn, and C. Becher, Coherent control and wave mixing in an ensemble of silicon-vacancy centers in diamond, *Phys. Rev. Lett.* **122**, 063601 (2019).
- [46] M.-A. Lemonde, V. Peano, P. Rabl, and D. G. Angelakis, Quantum state transfer via acoustic edge states in a 2d optomechanical array, *New J. Phys.* **21**, 113030 (2019).
- [47] L. Jiang, J. M. Taylor, A. S. Sørensen, and M. D. Lukin, Distributed quantum computation based on small quantum registers, *Phys. Rev. A* **76**, 062323 (2007).
- [48] M. Ruf, N. H. Wan, H. Choi, D. Englund, and R. Hanson, Quantum networks based on color centers in diamond, *J. Appl. Phys.* **130**, 070901 (2021).
- [49] C. T. Nguyen, D. D. Sukachev, M. K. Bhaskar, B. Machielse, D. S. Levonian, E. N. Knall, P. Stroganov, C. Chia, M. J. Burek, R. Riedinger, H. Park, M. Lončar, and M. D. Lukin, An integrated nanophotonic quantum register based on silicon-vacancy spins in diamond, *Phys. Rev. B* **100**, 165428 (2019).
- [50] M. K. Bhaskar, R. Riedinger, B. Machielse, D. S. Levonian, C. T. Nguyen, E. N. Knall, H. Park, D. Englund, M. Lončar, D. D. Sukachev, and M. D. Lukin, Experimental demonstration of memory-enhanced quantum communication, *Nature* **580**, 60 (2020).
- [51] C. Y. Hu, A. Young, J. L. O'Brien, W. J. Munro, and J. G. Rarity, Giant optical faraday rotation induced by a single-electron spin in a quantum dot: Applications to entangling remote spins via a single photon, *Phys. Rev. B* **78**, 085307 (2008).
- [52] M. Erhard, M. Krenn, and A. Zeilinger, Advances in high-dimensional quantum entanglement, *Nat. Rev. Phys.* **2**, 365 (2020).
- [53] Z. Xie, Y. Liu, X. Mo, T. Li, and Z. Li, Quantum entanglement creation for distant quantum memories via time-bin multiplexing, *Phys. Rev. A* **104**, 062409 (2021).
- [54] H. Zhou, T. Li, and K. Xia, Parallel and heralded multiqubit entanglement generation for quantum networks, *Phys. Rev. A* **107**, 022428 (2023).
- [55] B. Hensen, H. Bernien, A. E. Dréau, A. Reiserer, N. Kalb, M. S. Blok, J. Ruitenber, R. F. L. Vermeulen, R. N. Schouten, C. Abellán, W. Amaya, V. Pruneri, M. W. Mitchell, M. Markham, D. J. Twitchen, D. Elkouss, S. Wehner, T. H. Taminiau, and R. Hanson, Loophole-free bell inequality violation using electron spins separated by 1.3 kilometres, *Nature* **526**, 682 (2015).
- [56] S. Meesala, Y.-I. Sohn, B. Pingault, L. Shao, H. A. Atikian, J. Holzgrafe, M. Gündoğan, C. Stavarakas, A. Sipahigil, C. Chia, R. Evans, M. J. Burek, M. Zhang, L. Wu, J. L. Pacheco, J. Abraham, E. Bielejec, M. D. Lukin, M. Atatüre, and M. Lončar, Strain engineering of the silicon-vacancy center in diamond, *Phys. Rev. B* **97**, 205444 (2018).

- [57] B. Machielse, S. Bogdanovic, S. Meesala, S. Gauthier, M. J. Burek, G. Joe, M. Chalupnik, Y. I. Sohn, J. Holzgrafe, R. E. Evans, C. Chia, H. Atikian, M. K. Bhaskar, D. D. Sukachev, L. Shao, S. Maity, M. D. Lukin, and M. Lončar, Quantum interference of electromechanically stabilized emitters in nanophotonic devices, *Phys. Rev. X* **9**, 031022 (2019).
- [58] W. Dür and H.-J. Briegel, Stability of macroscopic entanglement under decoherence, *Phys. Rev. Lett.* **92**, 180403 (2004).
- [59] L. Aolita, D. Cavalcanti, A. Acín, A. Salles, M. Tiersch, A. Buchleitner, and F. de Melo, Scalability of greenberger-horne-zeilinger and random-state entanglement in the presence of decoherence, *Phys. Rev. A* **79**, 032322 (2009).
- [60] D. D. Sukachev, A. Sipahigil, C. T. Nguyen, M. K. Bhaskar, R. E. Evans, F. Jelezko, and M. D. Lukin, Silicon-vacancy spin qubit in diamond: A quantum memory exceeding 10 ms with single-shot state readout, *Phys. Rev. Lett.* **119**, 223602 (2017).
- [61] J. Borregaard, H. Pichler, T. Schröder, M. D. Lukin, P. Lodahl, and A. S. Sørensen, One-way quantum repeater based on near-deterministic photon-emitter interfaces, *Phys. Rev. X* **10**, 021071 (2020).